

https://doi.org/10.1070/QEL17146

Longitudinal spatial hole burning in high-power semiconductor lasers: numerical analysis

V.S. Golovin, I.S. Shashkin, S.O. Slipchenko, N.A. Pikhtin, P.S. Kop'ev

Abstract. **Longitudinal spatial hole burning (LSHB) in high-power semiconductor lasers is analysed by numerically solving one-dimensional (1D) rate equations. Calculations are performed for GaAs-based lasers operating at a wavelength of 1.06 μm. It is shown that the LSHB-induced decrease in output power can be accounted for by two mechanisms: build-up of spontaneous recombination and decrease in slope efficiency, equivalent to a rise in internal optical loss. We analyse the influence of different laser chip parameters on the magnitude of the LSHB effect. In particular, it is shown that to suppress LSHB it is preferable to increase the optical confinement factor Γ. We examine the relationship between LSHB and other mechanisms capable of reducing the output power.**

Keywords: *semiconductor laser, longitudinal spatial hole burning, rate equations, internal optical loss, numerical analysis.*

1. Introduction

High-power semiconductor lasers having a Fabry–Perot cavity and operating at wavelengths of ~1 μm are the most efficient light sources (with efficiency above 60%) [1–3]. To maximise their efficiency and output power, various mechanisms capable of degrading laser efficiency should be analysed in detail. One such mechanism – longitudinal spatial hole burning (LSHB) – is the subject of this study. This well-known effect [4–9] builds on a nonuniform carrier concentration distribution along the semiconductor laser cavity axis. In studies concerned with numerical simulation of light–current (L–I) characteristics of lasers, LSHB is usually regarded as a process that enhances other output power saturation mechanisms [10–13].

The direct effect of LSHB on laser slope efficiency was analysed by Avrutin and Ryvkin [9]. Their results demonstrate that, at high pump currents, the direct effect of LSHB can be described with sufficient accuracy using a single coefficient, f_{LSHB}, responsible for the relative increase in internal optical loss. As shown analytically and numerically, f_{LSHB} is to a first approximation only determined by the reflectivity of the output mirror, R_2, if the internal loss is considerably smaller than the output coupling loss and the reflectivity of the back mirror is $R_1 \approx 1$.

It was also shown by Avrutin and Ryvkin [9] that, at low currents, the dominant mechanism behind the LSHB-induced decrease in output power was the increase in spontaneous recombination current (effective threshold current). Because of the rather small decrease in power (by less than 5%), the LSHB effect has received relatively little attention, but according to our experimental data a transition from lasers with mirrors formed by cleaved facets (with $R_1 = R_2 \approx 0.3$ and negligible LSHB) to lasers with dielectric mirrors produced by sputter deposition often leads to a marked drop in slope efficiency at a given level of output coupling losses. Besides, the magnitude of the LSHB effect can depend significantly on the epitaxial design of lasers. It is therefore reasonable to conclude that the indirect effect of LSHB (enhancement of other mechanisms capable of reducing laser efficiency) can be important even at moderate pump currents. Thus, detailed analysis of LSHB is an important issue in designing high-power semiconductor lasers.

In most cases, output characteristics of high-power semiconductor lasers are determined using relations derived in a lumped zero-dimensional (0D) model [14]. In this work, 0D model applicability conditions are analysed in comparison with a 1D model that takes into account the LSHB effect.

2. Mechanism of the LSHB effect

Like in previous work [9], our analysis builds on rate equations describing the time-dependent balance between the electron concentration N_{e} in the active region and the lasing mode photon density N_{ph} in the waveguide. In the 0D approximation, the rate equations have the form

$$\frac{\mathrm{d}N_{\mathrm{e}}}{\mathrm{d}t} = \frac{\eta_{\mathrm{i}} I}{qV_{\mathrm{a}}} - R_{\mathrm{sp}}(N_{\mathrm{e}}) - v_{\mathrm{g}} g(N_{\mathrm{e}}) N_{\mathrm{ph}}, \tag{1}$$

$$\frac{\mathrm{d}N_{\mathrm{ph}}}{\mathrm{d}t} = \left[\Gamma v_{\mathrm{g}} g(N_{\mathrm{e}}) - \frac{1}{\tau_{\mathrm{ph}}}\right] N_{\mathrm{ph}}. \tag{2}$$

Here η_{i} is injection efficiency; I is the pump current; q is the elementary charge; $V_{\mathrm{a}} = d_{\mathrm{a}}WL$ is the active region volume; $R_{\mathrm{sp}} = AN_{\mathrm{e}} + BN_{\mathrm{e}}^2 + CN_{\mathrm{e}}^3$ is the spontaneous recombination rate; $v_{\mathrm{g}} = c/n_{\mathrm{eff}}$ is group velocity (where c is the speed of light in vacuum); $g(N_{\mathrm{e}}) = g_0 \ln(N_{\mathrm{e}}/N_{\mathrm{tr}})$ is the material gain; Γ is the optical confinement factor; $\tau_{\mathrm{ph}} = 1/[v_{\mathrm{g}}(\alpha_{\mathrm{i}} + \alpha_{\mathrm{m}})]$ is the photon lifetime in the cavity; and $\alpha_{\mathrm{m}} = (2L)^{-1} \ln(1/(R_1R_2))$ is the out-

V.S. Golovin, I.S. Shashkin, S.O. Slipchenko, N.A. Pikhtin, P.S. Kop'ev
Ioffe Institute, Russian Academy of Sciences, Politekhnicheskaya ul. 26, 194021 St. Petersburg, Russia;
e-mail: vsgolovin@mail.ioffe.ru

Received 1 October 2019
Kvantovaya Elektronika **50** (2) 147–152 (2020)
Translated by O.M. Tsarev

put coupling loss. The relation for α_m can be derived from the condition for the onset of lasing,

$$\Gamma\int_0^L [g(N_e) - \alpha_i]\,dz = \frac{1}{2}\ln\frac{1}{R_1 R_2},$$

in the $N_e(z)$ = const approximation. The parameters used in our calculations are listed below (z is a coordinate along the cavity axis):

Wavelength, λ/nm	1060
Active region thickness, d_a/nm	9
Stripe width, W/μm	100
Cavity length, L/μm	3000
Reflectivity of the back mirror ($z = 0$), R_1	0.95
Reflectivity of the output mirror ($z = L$), R_2	0.01
Injection efficiency, η_i	1.0
Shockley–Read–Hall recombination coefficient, A/s^{-1}	0
Radiative recombination coefficient, B/cm^3 s^{-1}	1×10^{-10}
Auger recombination coefficient, C/cm^6 s^{-1}	5×10^{-30}
Gain coefficient, g_0/cm^{-1}	2140
Transparency concentration, N_{tr}/cm^{-3}	1.77×10^{18}
Optical confinement factor, Γ	0.87×10^{-2}
Effective refractive index, n_{eff}	3.44
Internal optical loss, α_i/cm^{-1}	1.0

In the absence of any saturation mechanisms (so that α_i and η_i are constant and g is only determined by carrier concentration), the following relations for a steady-state ($dN_e/dt = dN_{ph}/dt = 0$) L–I characteristic of a laser can be derived from Eqns (1) and (2);

$$P = \eta(I - I_{th}), \tag{3}$$

$$\eta = \frac{E_{ph}}{q}\eta_i\frac{\alpha_m}{\alpha_m + \alpha_i}, \tag{4}$$

$$I_{th} = \frac{qV_a R_{sp}(N_{th})}{\eta_i}. \tag{5}$$

Here η is slope efficiency (the slope of the L–I curve); I_{th} is the threshold current; $E_{ph} = hc/\lambda$ is the photon energy (where h is the Planck constant); and N_{th} is the threshold electron concentration, which can be found from the relation $\Gamma g(N_{th}) = \alpha_i + \alpha_m$. Thus, the output power P is a linear function of pump current I.

In Eqns (1) and (2), N_e and N_{ph} are independent of spatial coordinates, i.e. longitudinal spatial hole burning is left out of account. To take into account this effect, it is necessary to turn to 1D rate equations:

$$\frac{\partial N_e}{\partial t} = \frac{\eta_i I}{qV_a} - R_{sp}(N_e) - v_g g(N_e)(N_{ph}^- + N_{ph}^+), \tag{6}$$

$$\frac{1}{v_g}\frac{\partial N_{ph}^-}{\partial t} = \frac{\partial N_{ph}^-}{\partial z} + [\Gamma g(N_e) - \alpha_i]N_{ph}^-, \tag{7}$$

$$\frac{1}{v_g}\frac{\partial N_{ph}^+}{\partial t} = -\frac{\partial N_{ph}^+}{\partial z} + [\Gamma g(N_e) - \alpha_i]N_{ph}^+, \tag{8}$$

where N_{ph}^+ and N_{ph}^- are the densities of photons moving in the $+z$ and $-z$ directions. Equations (7) and (8) are subject to the boundary conditions $R_1 N_{ph}^-(0) = N_{ph}^+(0)$ and $R_2 N_{ph}^+(L) = N_{ph}^-(L)$.

Consider now calculated L–I characteristics obtained by numerically solving 0D and 1D steady-state rate equations. If not stated otherwise, we give the total output optical power, i.e. we take into account emission from both sides of the Fabry–Perot cavity. Since rate equations are intended for describing laser operation above threshold, we used a minimum current $I = 1.05I_{th}$, and I_{th} was evaluated from (5). The parameters used (see above) correspond to a typical design of high-power semiconductor lasers operating at a wavelength $\lambda = 1.06$ μm [1, 2]. Gain as a function of electron concentration was described by a standard logarithmic function: $g(N_e) = g_0\ln(N_e/N_{tr})$. To find g_0 and N_{tr}, we used experimentally determined threshold current densities for different cavity lengths (L) and optical confinement factors (Γ).

Figure 1a shows light–current curves obtained with and without allowance for LSHB. It is seen that, in the 1D approximation, slope efficiency η is not constant (curve *3*). For $I \to I_{th}$, it tends to the 0D value, determined by (4). With increasing current, η drops sharply and has a minimum near threshold. At high pump currents, η stabilises. To interpret the shape of the $\eta(I)$ curve, we introduce the concepts of local slope efficiency (η') and local (or effective [8, 9]) threshold current (I'_{th}), defined as

$$\eta' = \frac{E_{ph}}{q}\eta_i\frac{N_{ph}^+(1 - R_2) + N_{ph}^-(1 - R_1)}{\Gamma\int_0^L g(N_e)(N_{ph}^+ + N_{ph}^-)\,dz}, \tag{9}$$

$$I'_{th} = \frac{qWd_a}{\eta_i}\int_0^L R_{sp}(N_e)\,dz. \tag{10}$$

In this case, locality is taken to imply that, using these quantities, an equivalent linear L–I curve described by Eqn (3) can be constructed for each point of a nonlinear L–I curve. The concepts of local threshold and local slope efficiency were first used by Golikova et al. [15] in analysing the saturation of measured L–I characteristics of cw lasers. Their physical meaning is as follows: to these threshold and slope efficiency values correspond the threshold concentration and optical loss of the semiconductor laser at a given operating point. Thus, we can separately consider two mechanisms behind the LSHB-induced decrease in output power: build-up of spontaneous recombination and increase in internal optical loss. Figure 1b shows calculated $\eta'(I)$ and $I'_{th}(I)$ curves.

Replacing η and I_{th} in (3) by η' and I'_{th}, we obtain the following relation for slope efficiency η in the 1D approximation:

$$\eta = \eta' + (I - I_{th})\frac{d\eta'}{dI} - \eta'\frac{dI'_{th}}{dI}. \tag{11}$$

It is the last term in the right-hand side of (11) which is responsible for the dip in the initial portion of the $\eta(I)$ curve. The rise in I'_{th} is also the main cause of the decrease in output power near threshold (Fig. 1c). At high currents, η' and I'_{th} stabilise and the output power is determined by η'.

Figure 2a illustrates the mechanism behind the increase in local threshold current I'_{th}. The strong nonuniformity of $N_e(z)$ leads to an increase in spontaneous recombination,

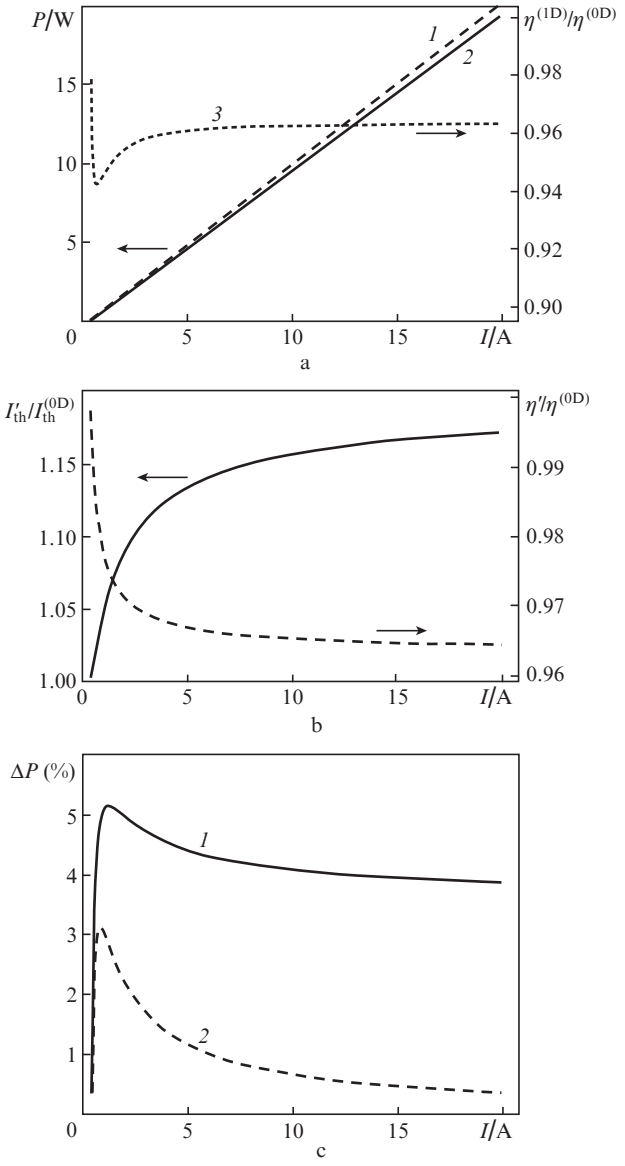

Figure 1. (a) Light–current curves obtained using rate equations in the 0D (1) and 1D (2) approximations and the ratio of the slopes of the curves (3); (b) ratios of the local threshold current I'_{th} and local slope efficiency η' to the values obtained in the 0D approximation; (c) total drop in output power in the 1D model (*1*) and the drop caused by the increase in local threshold current (*2*).

which can be regarded as an increase in effective electron concentration N'_e relative to threshold concentration N_{th}. The effective concentration is determined by the transcendental equation

$$R_{sp}(N'_e) = \frac{1}{L}\int_0^L R_{sp}(N_e)\,dz. \qquad (12)$$

The evolution of the shape of the $N_e(z)$ distribution with increasing current is well represented by the $I'_{th}(I)$ curve (Fig. 1b). Near the lasing threshold, $N_e \approx N_{th}$ at any point of the cavity. An increase in current leads to an increase in the density of photons, which begin to 'burn out' electrons near the output mirror. At high currents, the shape of $N_e(z)$ stabilises.

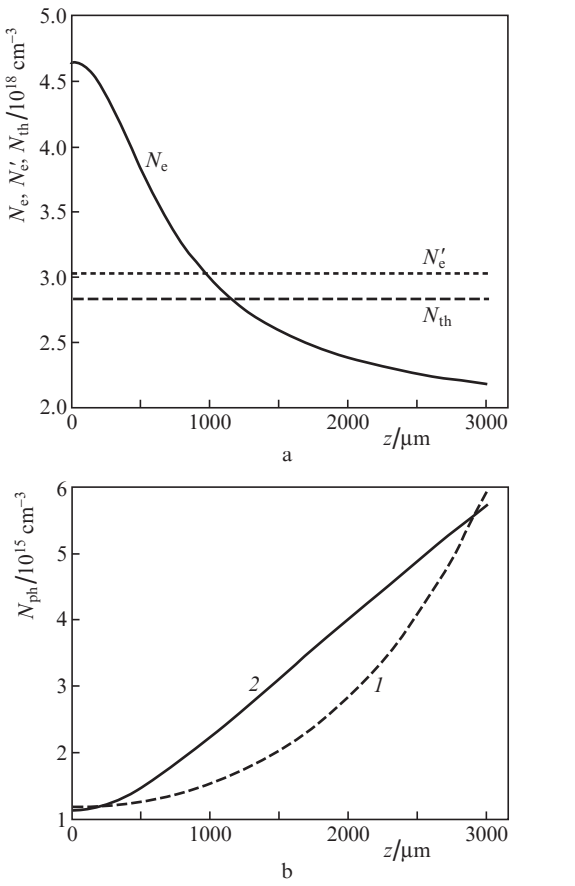

Figure 2. (a) Threshold electron concentration N_{th} in the absence of LSHB, electron concentration N_e distribution along the z-axis of the cavity with LSHB and effective electron concentration N'_e; (b) photon density N_{ph} distribution along the cavity axis (*1*) in the absence of and (*2*) with LSHB. Pump current $I = 10$ A.

As follows from (9), η' is determined by the photon density profile $N_{ph}(z)$. Figure 2b illustrates the effect of LSHB on this profile. Curve *1* is described by Eqns (7) and (8) provided the electron concentration is constant at $N_e = N_{th}$ along the z-axis (no LSHB) and the average photon density is

$$\langle N_{ph}\rangle \equiv \frac{1}{L}\int_0^L N_{ph}(z)\,dz = \frac{\eta_i I/(qV_q W) - R_{sp}(N_{th})}{g(N_{th})v_g}. \qquad (13)$$

In other words, electron concentration and average photon density are solutions to the system of Eqns (1) and (2). Curve *2* corresponds to a numerical solution to the system of Eqns (6)–(8). Clearly, LSHB increases the average photon density in the cavity, which is equivalent to a decrease in slope efficiency. Like in the case of electron concentration, the shape of $N_{ph}(z)$ sharply changes above threshold and stabilises at high currents, as evidenced by the $\eta'(z)$ curve (Fig. 1b).

3. Effect of laser design on LSHB

As mentioned above, to take into account LSHB in designing high-efficiency, high-power semiconductor lasers it is important to understand which laser parameters have a significant effect on LSHB. Consider first the influence of changes in cavity length L and output mirror reflectivity R_2 – two laser design parameters that are determined by the

final step of the fabrication process. The corresponding LSHB-induced relative power loss curves are presented in Fig. 3. The shape of the curves leads us to conclude that the cavity length has different effects on the above two mechanisms behind the decrease in output power: rise in I'_{th} and drop in η'. Increasing the output mirror reflectivity R_2 considerably reduces LSHB.

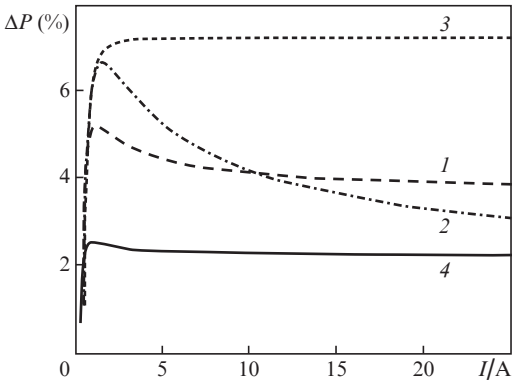

Figure 3. LSHB-induced drop in the output power of lasers with (*1*) $L = 3000$ μm and $R_2 = 1\%$, (*2*) $L = 1500$ μm and $R_2 = 1\%$, (*3*) $L = 6000$ μm and $R_2 = 1\%$, and (*4*) $L = 3000$ μm and $R_2 = 3\%$.

Figure 4 illustrates that it is important to take into account LSHB in choosing L and R_2: it shows regions of L and R_2 values that ensure the highest efficiency (above 99% of the maximum level) at a given output power. To map out these regions, an inverse problem was solved: we found the current necessary for obtaining a given output power. To convert the current to efficiency, we used the best fit plot of voltage against current density obtained from the measured current–voltage characteristics. It is seen that the distinction between the 0D and 1D models can be very significant. Thus, it is important to take into account LSHB in optimising the structure of lasers intended for operation at moderate output powers (about 1–10 W at $W = 100$ μm).

Consider now laser parameters that are determined by the epitaxial growth process. There is particular interest in the optical confinement factor Γ, because it depends on the waveguide design and the number of quantum wells and therefore can vary in a rather wide range. It is seen from Fig. 5 that Γ has a marked effect on LSHB and that it is preferable to increase it. Varying the gain coefficient g_0 leads to very similar results.

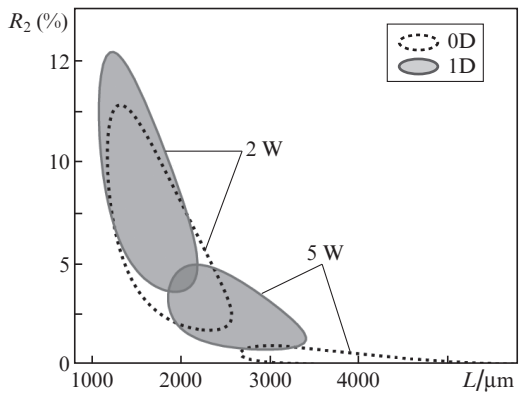

Figure 4. Regions of cavity lengths L and R_2 reflectivities that maximise efficiency at a given output optical power, obtained by solving 0D (without LSHB) and 1D (with allowance for LSHB) rate equations.

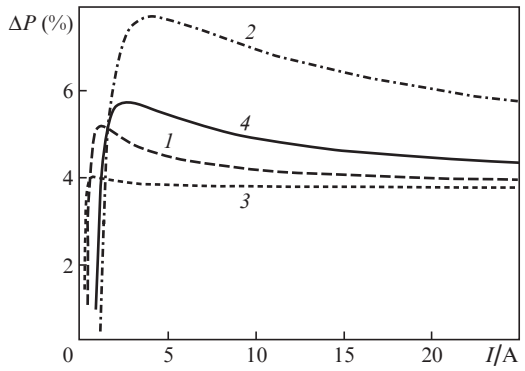

Figure 5. LSHB-induced drop in the output power of lasers with (*1*) $\Gamma = 0.87\%$ and $C = 5 \times 10^{-30}$ cm^6 s^{-1}, (*2*) $\Gamma = 0.43\%$ and $C = 5 \times 10^{-30}$ cm^6 s^{-1}, (*3*) $\Gamma = 1.74\%$ and $C = 5 \times 10^{-30}$ cm^6 s^{-1}, and (*4*) $\Gamma = 0.87\%$ and $C = 5 \times 10^{-29}$ cm^6 s^{-1}.

Comparison of curves *1* and *4* in Fig. 5 leads us to conclude that increasing the Auger recombination coefficient C leads to a larger drop in power in the initial portion of the L–I characteristic. The C value chosen by us for comparison is an order of magnitude higher than that used in our calculations (see Section 2), which corresponds to lasers operating at a wavelength $\lambda = 1.55$ μm. The radiative recombination coefficient B has a similar (but weaker) effect. To interpret these results, it is worth turning to previous work by Ryvkin and Avrutin [8], which demonstrates that the increase in I'_{th} is caused by nonlinear $g(N_e)$ and $R_{sp}(N_e)$ behaviour. Thus, the increase in the coefficients B and C or average electron concentration due to a decrease in Γ and g_0 leads to a rise in I'_{th}, as evidenced by the increase in both the height and width of the peak in the initial portion of the $\Delta P(I)$ curve.

At the same time, local slope efficiency η', which determines the slope of the L–I curve at high currents, is a very weak function of the epitaxial structure parameters considered above. It is determined primarily by the internal optical loss α_i. The $\Delta P(I)$ curves corresponding to $\alpha_i = 0.5$, 1.0 and 1.5 cm^{-1} are presented in Fig. 6a. It is seen that, at high currents, the relative LSHB-induced decrease in power, ΔP, is essentially proportional to α_i. This finding is important because the increase in internal optical loss as a result of the absorption by free charge carriers is thought to be the main mechanism behind the saturation of the L–I characteristic of high-power semiconductor lasers operating in pulsed mode [13, 16]. Figure 6b shows L–I curves calculated in the $\alpha_i = \alpha_i^0 + kJ$ approximation (where $k = 1.2 \times 10^{-4}$ cm A^{-1} and J is current density) [16, 17]. In this case, taking into account LSHB leads to an about 30% larger relative drop in output power as a result of the increase in α_i.

Another mechanism behind the decrease in output power, which is often interpreted in terms of LSHB, is carrier leakage into the waveguide [10, 18], which increases the absorption by

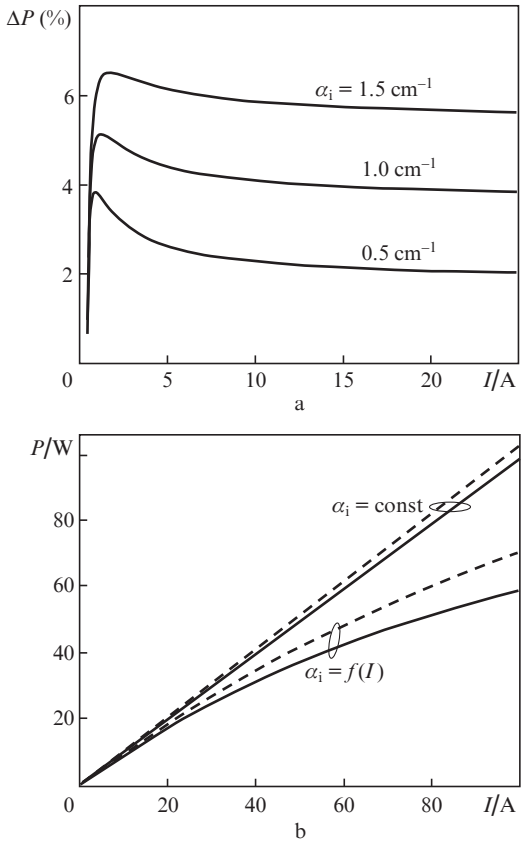

Figure 6. (a) LSHB-induced drop in the output power of lasers differing in α_i and (b) light–current curves calculated in the 0D (dashed lines) and 1D (solid lines) models at α_i = const and $\alpha_i = f(I)$.

free charge carriers and reduces injection efficiency η_i. Since the leakage is determined by not only the carrier concentration in the active region but also band bending [10, 13], it cannot be estimated in the model used in this study. We note only that comparison of Eqns (4) and (5) with (9) and (10) indicates that, in the case of η_i = const, the magnitude of η_i has no effect on LSHB.

Two-photon absorption (TPA) [19, 20] and gain saturation processes are also sometimes thought to be responsible for the saturation of the L–I characteristic of high-power semiconductor lasers. To a first approximation, two-photon absorption can be regarded as an increase in internal optical loss by $\alpha_{TPA} = \beta_{TPA}J(z)$, where β_{TPA} is the two-photon absorption coefficient and $J(z)$ is the local light intensity, proportional to the square of the photon density N_{ph}. Clearly, in this case taking into account nonuniformity of the photon distribution along the cavity axis has a strong effect on TPA. Indeed, for the laser design described in Section 2 and β_{TPA} = 20 cm GW^{-1}, a transition from the 0D to the 1D model led to an almost twofold increase in the TPA-induced relative drop in power. Gain saturation is, in turn, usually taken into account using the following modification to the gain function:

$$g(N_e, N_{ph}) = \frac{g(N_e)}{1 + \epsilon N_{ph}}, \qquad (14)$$

where ϵ is the gain saturation coefficient. In our calculations, we detected no correlation between LSHB and gain saturation, because these two mechanisms behind the decrease in output power were independent of each other.

4. Conclusions

The numerical analysis carried out in this work leads us to a number of conclusions as to the importance of taking into account the LSHB effect in designing high-power semiconductor lasers. In particular, as a result of LSHB the widely used 0D model of a laser [Eqns (1)–(5)] no longer provides accurate results even at moderate pump currents. An increase in error can be caused by low reflectivity of the output mirror, large internal optical losses, a low differential mode gain and a high spontaneous recombination rate.

One consequence of the distinction between the 0D and 1D models was illustrated in Fig. 4. At a given laser design, to each output power corresponds some optimal reflectivity of the output mirror, at which the pump current is lowest. In both the 1D and 0D cases, the optimal reflectivity tends to zero with increasing power, but this occurs at different rates.

Another problem related to the inaccuracy of the 0D model is that lasers with dielectric mirrors produced by sputter deposition differ in slope efficiency from lasers with mirrors formed by cleaved facets. The latter type of laser is typically used to determine the internal optical loss, the minimisation of which is a key issue in epitaxial design development. As a result of LSHB, however, lasers showing the best primary characterisation results, may have a considerably lower performance after mirrors are produced.

Taking into account LSHB is of greatest importance in modelling the saturation of L–I characteristics. To maximise the output power, use is typically made of lasers with a large cavity length and low reflectivity of their output mirror. Besides, one of the key mechanisms behind the saturation of L–I characteristics is often the growth of the internal optical loss, which is rather often minimised using structures with a 'thick' waveguide and, as a consequence, with a small optical confinement factor Γ. All these factors contribute to the LSHB effect, which enhances other saturation mechanisms.

Acknowledgements. This work was supported by the Russian Science Foundation (Grant No. 19-79-30072).

References

1. Pikhtin N.A., Slipchenko S.O., Sokolova Z.N., Stankevich A.L., Vinokurov D.A., Tarasov I.S., Alferov Zh.I. *Electron. Lett*., **40** (22), 1413 (2004).
2. Slipchenko S.O., Vinokurov D.A., Pikhtin N.A., Sokolova Z.N., Stankevich A.L., Tarasov I.S., Alferov Zh.I. *Semiconductors*, **38** (12), 1430 (2004) [*Fiz. Tekh. Poluprovodn*., **38** (12), 1477 (2004)].
3. Crump P., Erbert G., Wenzel H., Frevert C., Schultz C.M., Hasler K.-H., Staske R., Sumpf B., Maaßdorf A., Bugge F., Knigge S., Tränkle G. *IEEE J. Sel. Top. Quantum Electron*., **19** (4), 1501211 (2013).
4. Hasuo S., Ohmi T. *Jpn. J. Appl. Phys*., **13** (9), 1429 (1974).
5. Fang W.W., Bethea C.G., Chen Y.K., Chuang S.L. *IEEE J. Sel. Top. Quantum Electron*., **1** (2), 117 (1995).
6. Bennett A., Clayton R., Xu J. *J. Appl. Phys*., **83** (7), 3784 (1998).
7. Rinner F., Rogg J., Friedman P., Mikulla M., Weimann G., Poprawe R. *Appl. Phys. Lett*., **80** (1), 19 (2002).
8. Ryvkin B.S., Avrutin E.A. *J. Appl. Phys.*, **109** (4), 043101 (2011).
9. Avrutin E.A., Ryvkin B.S. *J. Appl. Phys*., **125** (2), 023108 (2019).

10. Wang X., Crump P., Wenzel H., Liero A., Hoffmann T., Pietrzak A., Schultz C.M., Klehr A., Ginolas A., Einfeldt S., Bugge F., Erbert G., Tränkle G. *IEEE J. Quantum Electron.*, **46** (5), 658 (2010).
11. Wenzel H., Crump P., Pietrzak A., Wang X., Erbert G., Tränkle G. *New J. Phys.*, **12** (8), 085007 (2010).
12. Zeghuzi A., Radziunas M., Wünsche H.-J., Klehr A., Wenzel H., Knigge A. *Opt. Quantum Electron.*, **50** (2), 88 (2018).
13. Piprek J., Li Z.-M. *IEEE Photonics Technol. Lett.*, **30** (10), 963 (2018).
14. Coldren L.A., Corzine S.W., Mašanović M.N. *Diode Lasers and Photonic Integrated Circuits* (Hoboken, NJ: John Wiley and Sons, 2012).
15. Golikova E.G., Kureshov V.A., Leshko A.Yu., Lyutetskiy A.V., Pikhtin N.A., Ryaboshtan Yu.A., Skrynnikov G.A., Tarasov I.S., Alferov Zh.I. *Semiconductors*, **34** (7), 853 (2000) [*Fiz. Tekh. Poluprovodn.*, **34** (7), 886 (2000)].
16. Veselov D.A., Kapitonov V.A., Pikhtin N.A., Lyutetskiy A.V., Nikolaev D.N., Slipchenko S.O., Sokolova Z.N., Shamakhov V.V., Shashkin I.S., Tarasov I.S. *Quantum Electron.*, **44** (11), 993 (2014) [*Kvantovaya Elektron.*, **44** (11), 993 (2014)].
17. Veselov D.A., Pikhtin N.A., Lyutetskiy A.V., Nikolaev D.N., Slipchenko S.O., Sokolova Z.N., Shamakhov V.V., Shashkin I.S., Kapitonov V.A., Tarasov I.S. *Quantum Electron.*, **45** (7), 597 (2015) [*Kvantovaya Elektron.*, **45** (7), 597 (2015)].
18. Ryvkin B.S., Avrutin E.A. *J. Appl. Phys.*, **97** (11), 113106 (2005).
19. Avrutin E.A., Ryvkin B.S. *Semicond. Sci. Technol.*, **32** (1), 015004 (2016).
20. Dogan M., Michael C.P., Zheng Y., Zhu L., Jacob J.H. *Proc. SPIE. High-Power Diode Laser Technology and Applications XII*, **8965**, 89650P (2014).